orbital is out of plane whereas the d_{xy} orbital is in plane. The first-principles calculations show a considerably enhanced magnetic moment for single-atom-thick Fe membranes (3.08 μB) as compared with bulk BCC Fe (2.1 μB), in good agreement with previously calculated values (*8*). The total magnetic moment is slightly decreased by the Fe-C boundary effect but is still much larger the bulk value (fig. S17).

In summary, the existence of free-standing monoatomic suspended Fe membranes is demonstrated. These 2D Fe nanomembranes are directly imaged and are shown to have a square lattice with a 2.65 Å lattice constant at room temperature. These studies provide valuable data for further more accurate and in-depth theoretical investigations. The potential of perforated graphene as a support for 2D membranes is shown, and one can anticipate new 2D structures from a variety of elements to emerge.

References and Notes

1. K. S. Novoselov *et al.*, *Science* **306**, 666–669 (2004).
2. C. H. Jin, F. Lin, K. Suenaga, S. Iijima, *Phys. Rev. Lett.* **102**, 195505 (2009).
3. H. Komsa, A. V. Krasheninnikov, *J. Phys. Chem. Lett.* **3**, 3652–3656 (2012).
4. D. Qian, X. F. Jin, J. Barthel, M. Klaua, J. Kirschner, *Phys. Rev. Lett.* **87**, 227204 (2001).
5. G. Wedler, C. M. Schneider, A. Trampert, R. Koch, *Phys. Rev. Lett.* **93**, 236101 (2004).
6. H. Ohnishi, Y. Kondo, K. Takayanagi, *Nature* **395**, 780–783 (1998).
7. M. J. Lagos, F. Sato, D. S. Galvão, D. Ugarte, *Phys. Rev. Lett.* **106**, 055501 (2011).
8. J. Izquierdo *et al.*, *Phys. Rev. B* **61**, 13639–13646 (2000).
9. R. Lorenz, J. Hafner, *Phys. Rev. B* **54**, 15937–15949 (1996).
10. W. Lu, K. Zhang, X. Xie, *Phys. Rev. B* **48**, 18159–18163 (1993).
11. J. G. Gay, R. Richter, *Phys. Rev. Lett.* **56**, 2728–2731 (1986).
12. M. Wuttig, J. Thomassen, *Surf. Sci.* **282**, 237–245 (1993).
13. A. Lehnert *et al.*, *Phys. Rev. B* **82**, 094409 (2010).
14. A. W. Robertson *et al.*, *Nano Lett.* **13**, 1468–1475 (2013).
15. O. Cretu *et al.*, *Phys. Rev. Lett.* **105**, 196102 (2010).
16. A. V. Krasheninnikov, P. O. Lehtinen, A. S. Foster, P. Pyykkö, R. M. Nieminen, *Phys. Rev. Lett.* **102**, 126807 (2009).
17. H. Wang *et al.*, *Sci. Rep.* **2**, 995 (2012).
18. F. Börrnert *et al.*, *J. Microsc.* **249**, 87–92 (2013).
19. B. Dai *et al.*, *Nat. Commun.* **2**, 522 (2011).
20. Y. C. Lin *et al.*, *ACS Nano* **5**, 2362–2368 (2011).
21. J. P. Perdew, K. Burke, M. Ernzerhof, *Phys. Rev. Lett.* **77**, 3865–3868 (1996).
22. S. Stankov *et al.*, *Phys. Rev. Lett.* **99**, 185501 (2007).
23. G. Grimvall, B. Magyari-Köpe, V. Ozolins, K. A. Persson, *Rev. Mod. Phys.* **84**, 945–986 (2012).
24. Y. Matsuda, W. Deng, W. A. Goddard III, *J. Phys. Chem. C* **114**, 17845–17850 (2010).
25. Ç. Ö. Girit *et al.*, *Science* **323**, 1705–1708 (2009).
26. J. Li, I. S. Yip, *Handbook of Materials Modeling* (Kluwer Academic Publishers, Dordrecht, Netherlands, 2005).

Acknowledgments: J.Z. thanks the Deutscher Akademischer Austausch Dienst DAAD Foundation, and S.G. thanks the Deutsche Forschungsgemeinschaft (RU 1540/8-1). thanks the DFG (project PO 1602/1-1 to A.P.). This work was supported by the Institute of Basic Science (IBS) Korea. We also thank Y.-h. Luo (East China University of Science and Technology) for providing us with the Dmol3 code. We thank S. Melkhanova and J. Pang for the fabrication of the CVD-grown graphene. We thank the IFW Dresden for granting us use of their microscopy facilities.

Supplementary Materials

www.sciencemag.org/content/343/6176/1228/suppl/DC1
Materials and Methods
Supplementary Text
Figs. S1 to S17
Tables S1 and S2
References (*27*–*33*)

28 August 2013; accepted 19 February 2014
10.1126/science.1245273

Main-Group Compounds Selectively Oxidize Mixtures of Methane, Ethane, and Propane to Alcohol Esters

Brian G. Hashiguchi,[1]* Michael M. Konnick,[1] Steven M. Bischof,[1] Samantha J. Gustafson,[2] Deepa Devarajan,[2] Niles Gunsalus,[1] Daniel H. Ess,[2]* Roy A. Periana[1]*

Much of the recent research on homogeneous alkane oxidation has focused on the use of transition metal catalysts. Here, we report that the electrophilic main-group cations thallium(III) and lead(IV) stoichiometrically oxidize methane, ethane, and propane, separately or as a one-pot mixture, to corresponding alcohol esters in trifluoroacetic acid solvent. Esters of methanol, ethanol, ethylene glycol, isopropanol, and propylene glycol are obtained with greater than 95% selectivity in concentrations up to 1.48 molar within 3 hours at 180°C. Experiment and theory support a mechanism involving electrophilic carbon-hydrogen bond activation to generate metal alkyl intermediates. We posit that the comparatively high reactivity of these d^{10} main-group cations relative to transition metals stems from facile alkane coordination at vacant sites, enabled by the overall lability of the ligand sphere and the absence of ligand field stabilization energies in systems with filled d-orbitals.

The world is undergoing a revolution in raw hydrocarbon feedstock supply with the discovery of increasingly abundant sources of natural gas in shale and offshore gas fields (*1*). Although natural gas is primarily methane, natural gas—particularly from shale—also has substantial amounts of ethane and propane (*2*). The conversion of methane, as well as these higher alkanes in natural gas, into liquid fuels and commodity chemicals such as methanol, ethylene, ethanol, ethylene glycol, isopropanol, and propylene glycol at lower costs than the current multistep, capital-intensive processes could reduce emissions and our dependence on petroleum, as well as increase the value of natural gas.

An important approach that has emerged in the past few decades is the design of molecular (homogeneous) catalysts for the oxidative functionalization of alkanes based on the CH activation reaction. This involves selective reaction of an M-X catalyst with a hydrocarbon CH bond (R-H) under relatively mild conditions without the involvement of radicals in order to generate a M-R intermediate that is converted to the desired R-X product with regeneration of M-X (Eq. 1). There has been considerable effort in this area of research with homogeneous (*3*–*23*) as well as heterogeneous catalysts (*24*–*26*), and substantial progress has been made in recent years. Most of the work on the homogeneous systems have been primarily based on transition metals (with unfilled d-shells, $d^{<10}$) such as Pt (*3*, *4*, *16*), Pd (*14*, *17*–*19*, *23*), Rh (*20*–*22*), and Ir (*7*–*10*). In contrast, relatively few studies have been directed toward the classic main-group elements with a filled d-shell (d^{10}). In 1993, we reported an example of a main-group metal cation, Hg^{II}, in the superacid concentrated H_2SO_4 for direct conversion of methane to methanol esters (*15*). In spite of the simplicity of the Hg^{II} system, it was not further developed because of lack of reaction in more practical, weaker acid media such as CF_3CO_2H (TFAH), CH_3CO_2H (HOAc), or aqueous acids with which product separation could be practical. Another key issue was that the reactions of ethane and propane were unselective with the Hg^{II} system. We originally proposed an electrophilic CH activation mechanism for the Hg^{II} system. However, later work by Sen, based on the observation of products resulting from C-C cleavage reactions with higher alkanes, suggested that Hg(II) in superacid media was sufficiently oxidizing to initiate free-radical reactions (*5*)

$$\text{M-X} + \text{R-H} \rightarrow \text{M-R} \rightarrow \text{M-X} + \text{R-X} \qquad (1)$$

This possibility for unselective radical reactions with higher alkanes was also considered by Moiseev and co-workers in the early 1990s on the reaction of alkanes in TFAH with strongly oxidizing salts that were known to be effective for oxidizing hydrocarbons through free-radical mechanisms (*27*, *28*). The initial report showed high yield and selectivity for the stoichiometric reactions of Co^{III} with methane to Me-TFA (*27*). Carrying out

[1]The Scripps Energy and Materials Center, Department of Chemistry, The Scripps Research Institute, Jupiter, FL 33458, USA. [2]Department of Chemistry and Biochemistry, Brigham Young University (BYU), Provo, UT 84602, USA.

*Corresponding author. E-mail: rperiana@scripps.edu (R.A.P.); dhe@chem.byu.edu (D.H.E.); bhashigu@scripps.edu (B.G.H.)

the reaction with Co^{II} in the presence of O_2 showed a turn over number (TON) of ~4 for Me-TFA, along with comparable amounts of CO_2 generated through solvent decarboxylation. Along with Co^{IV} peroxo species, both radical and nonradical mechanisms were considered. In a later report that focused on the reactions of ethane and propane, the authors proposed a free-radical mechanism to account for the extensive C-C cleavage and overoxidation reactions with these higher alkanes. In addition to transition metal salts, there was one table entry in (*28*) on the reaction of methane with stoichiometric amounts of a main-group d^{10} cation, Pb^{IV}, that generated Me-TFA in ~10% yield. The higher alkanes were not examined in that initial work, and there are no follow-up reports by Moiseev, suggesting that Pb^{IV} operated by a different mechanism from the radical reactions proposed for Co^{III}. In our own work on Hg^{II}, the main-group d^{10} cation, Tl^{III}, was also found to be active for methane oxidation to the ester. However, this was only examined in superacid media and only with methane. We did not further examine on the Tl^{III} or Pb^{IV} systems in TFAH or with higher alkanes. The primary basis for this was the recognition that both Tl^{III} with a standard reduction potential (E^o) of 1.2 V and Pb^{IV} (E^o = 1.5 V) are stronger oxidants than is Hg^{II} (E^o = 0.9 V) (*29*). Consequently, on the basis of the general considerations at that time we considered that these main-group cations would be more likely than would Hg^{II} to initiate unselective radical reaction with the higher alkanes. To our knowledge, since those early publications in the 1990s there are no reported, deliberate studies of reactions of higher alkanes with those or other strongly oxidizing main-group electrophiles.

Our later work with Pt^{II} also led to models that directed our efforts away from these main-group systems. In 1998, we reported that the well-defined transition metal complex [η-2-(2,2′-bipyrimidyl)]platinum(II), $(bpym)Pt^{II}X_2$ when dissolved in superacid solvents such as concentrated H_2SO_4 (*16*) was an effective catalyst for the functionalization of methane to ~1 M protonated methanol and bisulfate ester. However—along with the high cost of Pt, as was the case for Hg^{II}—this system was inactive in more practical,

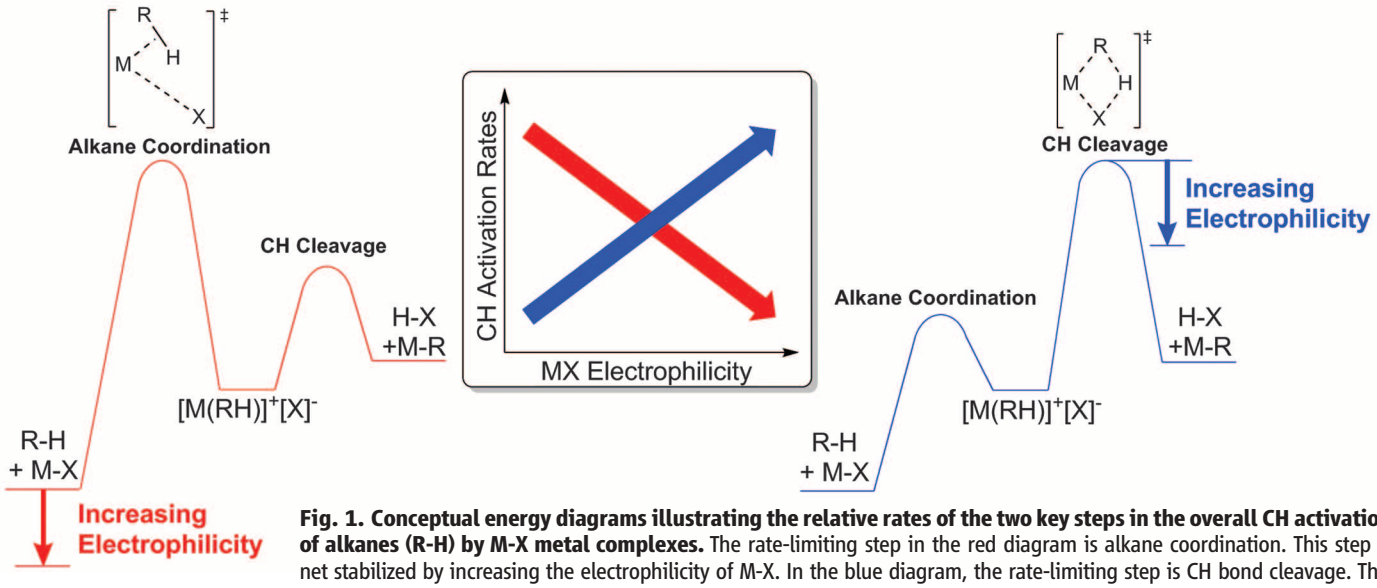

Fig. 1. Conceptual energy diagrams illustrating the relative rates of the two key steps in the overall CH activation of alkanes (R-H) by M-X metal complexes. The rate-limiting step in the red diagram is alkane coordination. This step is net stabilized by increasing the electrophilicity of M-X. In the blue diagram, the rate-limiting step is CH bond cleavage. This transition state is net stabilized by increasing the M-X electrophilicity. (Inset) The predicted trends in overall rate of CH activation with increasing electrophilicity of M-X for these cases are shown color-coordinated.

Table 1. Reaction of oxidants with methane, ethane, and/or propane. Standard conditions were 0.25 M $Tl(TFA)_3$ or $Pb(TFA)_4$ in 2 ml TFAH, gas pressure (MeH = 3.44 MPag, EtH = 3.44 MPag, or PrH = 0.861 MPag), 180°C for 3 hours. Conc (M), (moles oxidant)/(liters solvent added); product selectivity, [individual liquid product]/[total liquid products] × 100; yield based on ^{1}H-NMR, [oxidant]/[total liquid products] × 100; and [product], (moles product)/(liters solvent added).

Entry	Oxidant	Conc (M)	Solvent	Hydrocarbon	Products (% of total products)	Yield ([product])
1	$Tl(TFA)_3$	0.250	HTFA	MeH	MeTFA (100%)	74% (0.19 M)
2*	$Tl(TFA)_3$	2	HTFA	MeH	MeTFA (100%)	55% (1.1 M)
3	$Tl(TFA)_3$	0.250	HTFA	EtH	EtTFA (67%), $EG(TFA)_2$ (33%)	75% (0.16 M)
4	$Tl(TFA)_3$	3	HTFA	EtH	EtTFA (64%), $EG(TFA)_2$ (36%)	60% (1.48 M)
5	$Tl(TFA)_3$	0.250	HTFA	PrH	iPrTFA (77%), $PG(TFA)_2$ (23%)	>95% (>0.22 M)
6	$Tl(TFA)_3$	0.250	HTFA	100(MeH): 8(EtH):1(PrH)†	MeTFA (9%), EtTFA (21%), $EG(TFA)_2$ (11%), iPrTFA (10%), $PG(TFA)_2$ (19%)	82% (0.11 M)
7‡	$Tl(TFA)_3$	0.250	HTFA/H_2O	EtH	EtTFA (68%), $EG(TFA)_2$ (32%)	73% (0.16 M)
8§	$Tl(TFA)_3$	0.250	HTFA	EtH	EtTFA (66%), $EG(TFA)_2$ (34%)	76% (0.16 M)
9‖	$Tl(TFA)_3$	0.250	HTFA	EtH	EtTFA (65%), $EG(TFA)_2$ (35%)	30% (0.06 M)
10	$Tl(TFA)_3$	0.250	MSA	EtH	EtX (47%), $EG(X)_2$ (53%)¶	93% (0.18 M)
11	$Tl(OAc)_3$	0.250	HOAc	EtH	EtOAc (2%), $EG(OAc)_2$ (98%)	43% (0.06 M)
12	$Pb(TFA)_4$	0.250	HTFA	MeH	MeTFA (100%)	76% (0.19 M)
13	$Pb(TFA)_4$	0.250	HTFA	EtH	EtTFA (70%), $EG(TFA)_2$ (30%)	90% (0.2 M)
14‖	$Pb(TFA)_4$	0.250	HTFA	EtH	EtTFA (68%), $EG(TFA)_2$ (32%)	75% (0.18 M)
15	$Hg(TFA)_2$	0.250	HTFA	EtH	N/A	0% (0.0 M)

*Pressure, 5.52 MPag; and temperature (*T*) = 190°C. †Total pressure, 3.44 MPag. ‡Run with 2 M H_2O present. §Run with 100 kPa O_2 present. ‖Reactions were run at 150°C. ¶Products were a mixture of EtTFA, Et(MSA), $EG(TFA)_2$, and $EG(MSA)_2$.

weaker acids as well as unselective for reaction with higher alkanes. Studies suggested that this system operated by means of electrophilic CH activation and that the lack of reaction in weaker non-superacid solvents resulted from effectively complete inhibition of the CH activation step in these media (*30*). As shown conceptually in Fig. 1, electrophilic CH activation by M-X transition metal complexes are typically considered to proceed through two general steps, involving (i) alkane R-H coordination to M-X to generate $[M(R\text{-}H)]^+ + X^-$ followed by (ii) CH bond cleavage to generate M-R. Studies show that CH activation by the (bpym)Pt system operates as described with the red diagram in Fig. 1, in which R-H coordination is rate limiting, and inhibition in moving from superacid to weaker acid solvents results from stronger coordination of the more nucleophilic anions, X^-, present in weaker acid solvents to the electrophilic metal center. This results in net stabilization of the M-X resting state and increases the barrier to R-H coordination and CH activation.

At the time of these discoveries, we erroneously considered that all electrophilic CH activation systems would operate as in the model shown in red in Fig. 1. Consequently, we assumed that stabilization of the resting state also accounted for the inhibition of Hg^{II} in weaker, non-superacid media as well as the counterintuitive observations, in both the (bypm)Pt and Shilov PtCl systems, that the higher oxidation state Pt^{IV} is effectively inactive, whereas lower-oxidation-state Pt^{II} exhibits high rates of electrophilic CH activation. For systems operating as described with the red energy diagram in Fig. 1, it could be expected that the relative rate of CH activation would decrease with increasing electrophilicity (Fig. 1, inset, red arrow). Between this resting-state stabilization model and concerns of possible radical reactions, our studies were directed away from Tl^{III}, Pb^{IV}, and other main group cations that were more strongly oxidizing and electrophilic than are Pt^{II} (E^o = ~0.8 V) (*29*) and Hg^{II} for functionalization of higher alkanes in more practical, weaker acid media.

Contrary to those predictions, we now find that $Tl^{III}(TFA)_3$ and $Pb^{IV}(TFA)_4$ can rapidly functionalize methane, ethane, and propane separately or as mixtures, in high selectivity and concentrations to the corresponding trifluoroacetate esters of methanol (MeTFA), ethanol (EtTFA), ethylene glycol [$EG(TFA)_2$], isopropanol (iPrTFA), and 1,2-propylene glycol [$PG(TFA)_2$] (Table 1, entries 1 to 6, 8, 9, and 12 to 15). We focused primarily on TFAH as the reaction medium but also observed efficient reactivity in other non-superacidic solvents, such as methane sulfonic acid (MSA) (Table 1, entry 10), HOAc (Table 1, entry 11), and TFAH/H_2O mixtures (Table 1, entry 7). In contrast to the reported reactions with $(bpym)Pt^{II}$ or Hg^{II} in superacid media, no evidence for C-C cleavage or other side products were observed with the higher alkanes, ethane and propane. In spite of the original concerns of radical reactions and inhibition of CH activation in non-super acid media, we nonetheless believe it is plausible to rationalize the reactions of these nontransition metal, main-group d^{10} cations with alkanes by means of a general reaction mechanism involving electrophilic CH activation and M-R functionalization, which have primarily been associated with transition metals.

Some of the earliest studies on ligand interaction with metal cations show that the rates of ligand exchange for the third row, main-group, d^{10} strong electrophiles such as Hg^{II} and Tl^{III} are ~10^{19} faster than for the transition metal $d^{<10}$ cations such as Ir^{III} or Pt^{IV}. (*31*) These extraordinary differences in rate are conceptually attributed to lack of ligand field stabilization energies (LFSE) for cations with filled d-orbitals and strong LFSE for cations with unfilled d-orbitals. On the basis of these enormous differences in exchange rates, it is plausible that the rate of alkane coordination for main-group d^{10} electrophiles could be fast and that CH bond cleavage could be comparatively slow and rate limiting (Fig. 1, blue lines) for the overall CH activation process. It is also plausible that with this switch in the rate-limiting step, increasing electrophilicity could result in a net lowering of the transition state for CH bond cleavage. This can be explained by hard soft acid base (HSAB) theory, in which an increase in the M-C bond strength would be expected with increasing electrophilicity of these soft polarizable, third-row d^{10} electrophiles (*32*). As shown in Fig. 1, these considerations lead to the prediction that the rate of electrophilic CH activation (Fig. 1, inset, blue arrow) with these main-group d^{10} cations could increase with increasing electrophilicity (assuming that alkane coordination continues to be fast). This is opposite to the trend in our earlier model (Fig. 1, inset, red arrow). Counterintuitively, this new model suggests that the lack of reaction of Hg^{II} in weaker acid media was because its electrophilicity was too low rather than too high. These considerations led us to more closely examine the reaction mechanism of the Tl^{III}-mediated alkane oxidation.

The crude mixtures from the reactions of Tl^{III} with the alkane in TFAH are homogeneous and effectively colorless. The ^{1}H–nuclear magnetic resonance (NMR) spectra of the crude reaction mixtures in TFAH from separate reactions of 3.44 MPag of methane and ethane, and 0.861 MPag of propane with $Tl(TFA)_3$ in CF_3CO_2H solvent at 180°C for 3 hours are shown in Fig. 2, A to C. A coaxial insert was used as an external standard. The TFA-ester of methanol (MeTFA) and the corresponding esters of ethanol (EtTFA) and ethylene glycol [$EG(TFA)_2$] are the only products observed (within a 1% detection threshold) from methane and ethane, respectively. The reaction with propane (Table 1, entry 5) is also very efficient and only generates the corresponding esters of isopropanol (iPrTFA) and 1,2-propylene glycol [$PG(TFA)_2$]. Reactions conducted with 100% ^{13}C-labeled methane ($^{13}CH_4$) and ethane ($^{13}C_2H_6$) unambiguously confirmed that the esters are formed from the corresponding alkanes. Exclusively ^{13}C-labeled products were observed in the liquid phase, and only traces of $^{13}CO_2$ were detected in the gas phase. No products from C-C cleavage or other side reactions were observed in the liquid phases. Consistent with this high selectivity, control studies showed that the ester

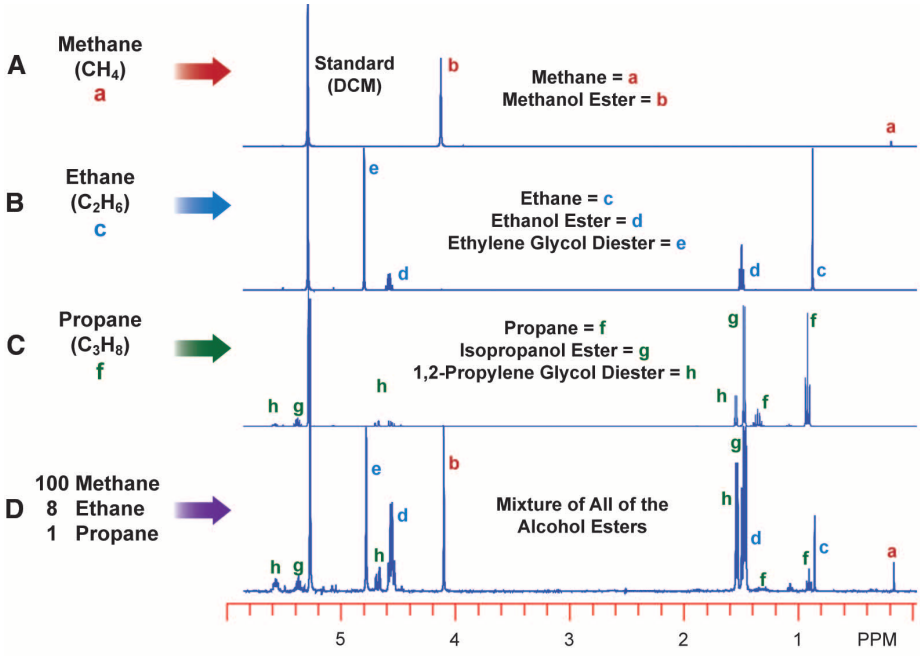

Fig. 2. Stacked ^{1}H-NMR (400 MHz) spectra of the crude reaction mixtures in TFAH after Tl^{III}–mediated oxidation of alkanes. The alkanes were, respectively, (**A**) methane, (**B**) ethane, (**C**) propane, and (**D**) a mixture of methane, ethane, and propane in a ratio typical in natural gas. The products are the alcohol esters of trifluoroacetic acid.

products are unreactive toward $Tl(TFA)_3$ when the hydrocarbon gas is replaced with argon under otherwise identical conditions. Assuming a detection limit of ~1% and a 5 mM methane concentration in the liquid phase, the parent alkanes appear to be at least 100 times more reactive than are the alcohol ester products. Because the TFA group is electron-withdrawing relative to a H atom, this is consistent with an electrophilic reaction with the CH bonds in which positive charge is developed on the carbon during CH cleavage.

Consistent with the 1:1 metal:alkane stoichiometry shown in Eq. 2, analysis of a crude reaction mixture with ethane by means of Tl-NMR before and after a reaction shows unreacted Tl^{III} as well as Tl^{I} (fig. S7). Increasingly abundant shale gas contains, in addition to methane, substantial amounts of ethane and propane. To examine whether these alkanes could be functionalized without separation in a one-pot procedure, we prepared and examined the reaction of a mixture of methane, ethane, and propane in a 100:8:1 ratio typical in natural gas. As can be seen from ^{1}H and ^{13}C-NMR analysis of the crude reaction mixture in TFAH (Fig. 2D), each alkane is converted to the corresponding alcohol esters, in high selectivity in a molar ratio of MeTFA:[EtTFA + $EG(TFA)_2$]:[iPrTFA + $PG(TFA)_2$] of ~1:3:3. When normalized for the number of hydrogens in each of the alkanes, the relative reactivity of the CH bonds in methane, ethane, and propane is ~1:25:150. This trend is also consistent with an electrophilic reaction with the CH bonds that would be expected to proceed in the order of $CH_4 < CH_3\text{-}CH_3 < CH_3CH_2CH_3$ as H-atoms on CH_4 are replaced by more electron-donating CH_3 groups

$$\text{R-H} + Tl^{III}(TFA)_3 \rightarrow Tl^{I}(TFA) + \text{TFAH} + \text{R-TFA} \quad (2)$$

As discussed above, a prediction of the blue reaction model in Fig. 1 is that in contrast to our earlier model for electrophilic CH activation, the rates of alkane functionalization should increase with increasing electrophilicity. Indeed, under identical conditions—in the absence of mass transfer limitations and at shorter reaction times so as to minimize conversion of the salts—the total yield of EtTFA and $EG(TFA)_2$ from $Hg(TFA)_2$, $Tl^{III}(TFA)_3$, and $Pb^{IV}(TFA)_4$ was 0, 30, and 75%, respectively (Table 1, entries 14, 9, and 13, respectively). In (*27*), the one data entry on the reaction of Pb^{IV} with methane in TFAH shows ~10% methanol ester yield. Compared with our result of 74% yield with $Tl^{III}(TFA)_3$ (Table 1, entry 1), this would conflict with our model because it would suggest that Tl^{III} is more reactive than Pb^{IV} is. However, we find that the yield from the reaction of methane with $Pb(TFA)_4$ is reproducibly, considerably higher (>70 versus 10%) (Table 1, entry 12). At this time, we do not understand the basis for this difference. Our results qualitatively show that the relative rates of reactivity of these electrophiles with ethane in TFAH is Hg^{II} (inactive) << $Tl^{III} < Pb^{IV}$. If the trend holds through this third-row d^{10} series, it is possible that Bi^{V} could be very reactive with alkanes. $Bi^{V}(TFA)_5$ as well as $Au^{I}(TFA)$ are unknown, and efforts are underway to synthesize and study these species.

These observations support a proposed electrophilic CH activation/M-R functionalization mechanism. However, given the general consideration that strongly oxidizing species can generate free-radical reactions with alkanes, we were prompted to carry out further mechanistic studies. Varying the alkane pressure shows a first-order rate dependence [observed rate constant (k_{obs}) = $2.6 \times 10^{-6} \pm 1.3 \times 10^{-7}$ s^{-1} MPa^{-1}] on alkane (fig. S7). Some key characteristics of free-radical reactions can be, but not always, poor reproducibility and changes in reaction rate and product selectivity in the presence of radical traps, such as O_2 (*28*). To examine these possibilities, we studied the kinetics for the reaction of $Tl(TFA)_3$ with a 33-fold excess of ethane in TFAH. The reaction exhibits highly reproducible, clean, first-order (in Tl^{III}) kinetics ($k_{obs} = 9.0 \times 10^{-5} \pm 4.5 \times 10^{-6}$ s^{-1} MPa^{-1}) for the generation of the TFA esters of EtTFA and $EG(TFA)_2$, with no induction period (fig. S9). The rate of formation of EtTFA is higher than $EG(TFA)_3$, but as can be seen in fig. S9, the ratio of [EtTFA] to [$EG(TFA)_2$] is constant as the reaction proceeds. This would suggest that these materials are generated in parallel rather than sequentially [EtH to EtTFA to $EG(TFA)_2$] as might be expected. Consistent with this control, experiments show that conversion of EtTFA to $EG(TFA)_2$ is slow in the presence of $Tl(TFA)_3$. In contrast, ethylene is found to rapidly convert to $EG(TFA)_2$ in the presence of $Tl(TFA)_3$. This could suggest that ethylene is the precursor to $EG(TFA)_2$ and is generated in parallel with EtTFA (scheme S2). These results would suggest a common intermediate—plausibly, a Tl^{III}-Et species—for the parallel formation of both products (Fig. 3, scheme S2, and fig. S9). Carrying out the reaction in the presence of added O_2 (a well-known radical trap that is stable under these reaction conditions) had no effect on the reaction rate or selectivity (Table 1, entry 8). These results—along with the high reaction selectivity and lack of any C-C cleavage products in the reaction of ethane and propane with $Tl(TFA)_3$—strongly argue against a free-radical mechanism.

To further investigate the possibility of a CH activation/M-R functionalization mechanism, we carried out the reaction of methane with $Tl(TFA)_3$ in deuterated trifluoroacetic acid (DTFA). Only CH_3TFA was generated in this reaction, and no CH_3D was observed. This result would be consistent with a reaction mechanism in which CH activation step is rate-limiting and irreversible, whereas functionalization of the putative Tl^{III}-CH_3 intermediate to the alcohol ester is fast. Consistent with assignment of CH bond cleavage as the rate-limiting step, the intramolecular kinetic isotope effect (KIE) based on reactions with H_3C-CD_3 was measured to be 3.4. A very small KIE or no KIE would be expected if alkane coordination or M-R functionalization were rate-limiting. The expected putative $(TFA)_2Tl^{III}$-Me intermediate is

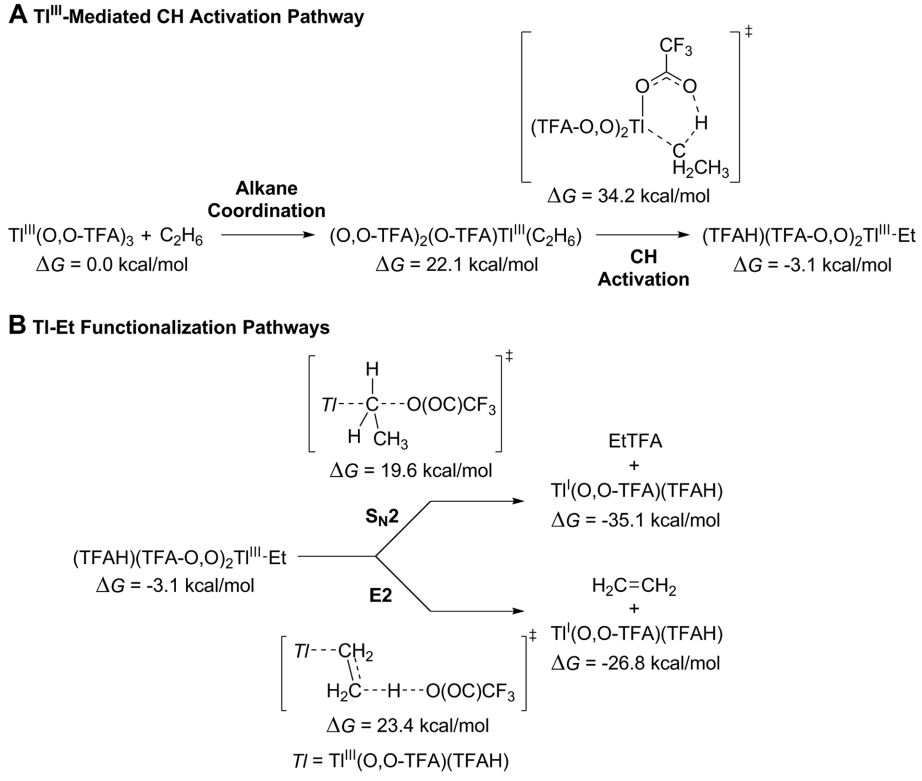

Fig. 3. M06/6-31+G(d,p)[LANL2DZ] DFT-calculated CH activation and M-R functionalization pathways in TFAH solvent.

unknown and likely unstable. However, the dimethyl species (TFA)Tl(CH_3)$_2$ is stable in TFAH at room temperature. Because this class of organometallic compounds are well known to undergo rapid alkyl transfer, we examined the reaction of (TFA)Tl(CH_3)$_2$ with Tl(TFA)$_3$ as a means of generating (TFA)$_2$Tl^{III}-Me in situ. Upon addition of Tl(TFA)$_3$ at room temperature to a solution of (TFA)Tl(CH_3)$_2$ in TFAH, within minutes two equivalents of MeTFA were cleanly generated in quantitative yield relative to (TFA)Tl(CH_3)$_2$ based on the stoichiometry shown in Eq. 3. Analysis of the crude reaction mixture by means of 1H-NMR immediately upon mixing showed a new, broad, transient Me-species that could be the (TFA)$_2$Tl(CH_3) intermediate. Consistent with the lack of H/D exchange in reactions of CH_4 with Tl(TFA)$_3$ in DTFA [which we attributed to irreversible formation of the putative (TFA)$_2$Tl^{III}-Me intermediate from CH activation], no CH_4 is generated from these functionalization reactions of (TFA)Tl(CH_3)$_2$ with Tl(TFA)$_3$ in TFAH. These results are also consistent with reports that treatment of (OAc)$_2$TlMe with HOAc generates MeOAc (*33*)

$$(\mathrm{TFA})\mathrm{Tl}^{\mathrm{III}}(\mathrm{CH_3})_2 + \mathrm{Tl}^{\mathrm{III}}(\mathrm{TFA})_3 \xrightarrow[\mathrm{TFAH}]{} 2\mathrm{MeTFA} + 2\mathrm{Tl}^{\mathrm{I}}(\mathrm{TFA}) \quad (3)$$

We have also used M06 density functional theory (DFT) calculations to examine possible mechanisms and the energy landscape for ethane CH functionalization, as well as to postulate a mechanism that accounts for the parallel formation of EtTFA and EG(TFA)$_2$. Calculation details can be found in the supplementary materials. To begin, we examined whether it is plausible that Tl(TFA)$_3$ can induce functionalization of ethane by a radical or one-electron oxidation pathway. Radical chain mechanisms beginning with a reactive (TFA)$_2$Tl•/CF_3COO•radical pair were ruled out because Tl-O bond homolysis requires 52.3 kcal mol^{-1} of free energy. Additionally, one-electron oxidation and Tl-mediated hydrogen atom abstraction were also ruled out because these pathways require greater than 75 kcal mol^{-1}. Instead, our calculations suggest that the most viable pathway for ethane CH functionalization is CH activation by means of electrophilic substitution (Fig. 3A). Calculations also suggest an identical mechanism for methane (supplementary materials).

In the ground state for Tl(O,O-TFA)$_3$, both oxygen atoms of the three TFA anions coordinate to the Tl center in an octahedral-like geometry, and one oxygen atom in each coordinated TFA is more tightly bound than the other. Ethane coordination requires dissociation of one oxygen atom in a O,O-TFA anion ligand to generate an open coordination site, to give (O,O-TFA)$_2$(O-TFA)Tl(C_2H_6). As anticipated from the conceptual model shown in Fig. 1 (blue energy diagram), ethane coordination requires a free energy change (ΔG) of 22.1 kcal mol^{-1}, in part because the d^{10} main group metal lacks LFSE. This ethane coordination energy in non-superacid solvent is much lower than the >35 kcal mol^{-1} value found for alkane coordination in superacid solvent with the d^8 (bpym)Pt^{II} system that has LFSE. Subsequent CH bond cleavage from (O,O-TFA)$_2$(O-TFA)Tl(C_2H_6) by means of an electrophilic substitution transition-state free energy change $\Delta G^{\ddagger}$ = 34.2 kcal mol^{-1} to generate (O,O-TFA)$_2$(TFAH)Tl-Et is consistent with the rates of reactions observed and with rate-limiting CH bond cleavage. Consistent with the experimentally measured KIE of 3.4, in this CH bond cleavage transition state there is considerable Tl-C bond formation and C-H bond stretching. Calculation of the KIE based on this transition state gave a value of 4.7. One prediction based on Fig. 1 is that Pb^{IV} should be more reactive than Tl^{III} is. Indeed, calculation of the electrophilic substitution transition state for Pb(O,O-TFA)$_4$ with ethane gave a lower $\Delta G^{\ddagger}$ of 29.2 kcal mol^{-1} (supplementary materials).

The thermodynamics for the CH activation step suggests that the Tl-Et species is more stable than are the Tl(TFA)$_3$ and ethane species (ΔG = –3.1 kcal mol^{-1}). Thus, a Tl-Et species such as (O,O-TFA)$_2$(TFAH)Tl-Et might be observable. However, calculations predict that Tl-Et functionalization has a much lower barrier than that of CH activation, and therefore, functionalization of the Tl-Et species is much more rapid than the CH activation reaction. This explains the lack of H/D exchange when the reactions are run in deuterated TFAD as well as the quantitative yield of MeTFA without any CH_4 formation from the reaction of (TFA)TlMe_2 with Tl(TFA)$_3$ in TFAH. Calculations suggest that there is parallel formation of EtTFA and EG(TFA)$_2$ from the Tl-Et intermediate. The two most plausible pathways for functionalization are shown in Fig. 3B. The S_N2 pathway forms EtTFA, whereas the E2 pathway forms ethylene. Control experiments show that although EtTFA conversion is slow, ethylene rapidly converts to EG(TFA)$_2$ in the presence of Tl(TFA)$_3$ (scheme S2). Thus, this E2 pathway leads to EG(TFA)$_2$. The calculations suggest that although the S_N2 and E2 pathways are competitive, there is a preference for the S_N2 pathway. This is consistent with experiments showing parallel but higher rates of formation of EtTFA relative to EG(TFA)$_2$.

Consistent with the proposed electrophilic CH activation mechanism and the experimental observations that MeTFA is less reactive than CH_4, the calculated $\Delta G^{\ddagger}$ for CH activation of MeTFA is ~9 kcal mol^{-1} higher than the $\Delta G^{\ddagger}$ for CH activation of CH_4 (supplementary materials). Calculations also reveal that the presence of the TFA electron-withdrawing group increases the activation barrier for CH activation of the methyl group of EtTFA to 40.4 kcal mol^{-1}. This suggests that the TFA group imparts a strong electron-withdrawing influence even two carbon atoms away. This result is consistent with the observed slow conversion of EtTFA to EG(TFA)$_2$. The electrophilic mechanism is also consistent with higher reactivity of ethane versus methane because methyl groups are electron-donating groups (calculations are available in the supplementary materials).

Experiment and theory taken together strongly support the proposed mechanism for alkane functionalization involving slow, irreversible electrophilic CH activation of alkanes with third-row, main-group cations, M^{n}X to generate M^n-R intermediates, followed by fast M-R functionalization to generate MeX and M^{n-2}. In the 1970 to 1980s, patented technologies were developed to reoxidize Tl^{I} to Tl^{III} by using O_2 in connection with Tl^{III}–mediated oxidation of olefins to glycols in HOAc (*34*–*36*). Applying this reoxidation technology to reactions of other main-group d^{10} cations, M^{n}X—with alkanes, either in two separate stoichiometric reactions or, ideally, with M^{n}X as a catalyst—could lead to practical processes for the selective hydroxylation of alkanes to alcohols by using air or other oxidants, such as H_2O_2. The absence of claims for reaction of ethane or other alkanes in these patented olefin oxidation technologies is most likely due to early beliefs that alkanes were inert to these main-group cations.

References and Notes

1. U. S. E. I. Administration, *U.S. Crude Oil and Natural Gas Proved Reserves* **2011**, 1–49 (2013).
2. D. L. George, E. B. Bowles Jr., *Pipeline Gas J.* **238**, 38–41 (2011).
3. N. F. Gol'dshleger, V. V. Es'kova, A. A. Shteinman, A. E. Shilov, *Russ. J. Phys. Ch. USSR* **46**, 785–786 (1972).
4. A. E. Shilov, A. A. Shteinman, *Coord. Chem. Rev.* **24**, 97–143 (1977).
5. A. Sen, *Acc. Chem. Res.* **31**, 550–557 (1998).
6. M. J. Burk, R. H. Crabtree, C. P. Parnell, R. J. Uriarte, *Organometallics* **3**, 816–817 (1984).
7. M. J. Burk, R. H. Crabtree, *J. Am. Chem. Soc.* **109**, 8025–8032 (1987).
8. M. C. Haibach, S. Kundu, M. Brookhart, A. S. Goldman, *Acc. Chem. Res.* **45**, 947–958 (2012).
9. J. Choi, A. H. R. MacArthur, M. Brookhart, A. S. Goldman, *Chem. Rev.* **111**, 1761–1779 (2011).
10. A. S. Goldman *et al.*, *Science* **312**, 257–261 (2006).
11. B. G. Hashiguchi, S. M. Bischof, M. M. Konnick, R. A. Periana, *Acc. Chem. Res.* **45**, 885–898 (2012).
12. C. J. Jones *et al.*, *Angew. Chem. Int. Ed.* **43**, 4626–4629 (2004).
13. R. A. Periana, O. Mironov, D. J. Taube, S. Gamble, *Chem. Commun. (Camb.)* **20**, 2376–2377 (2002).
14. R. A. Periana, O. Mironov, D. Taube, G. Bhalla, C. J. Jones, *Science* **301**, 814–818 (2003).
15. R. A. Periana *et al.*, *Science* **259**, 340–343 (1993).
16. R. A. Periana *et al.*, *Science* **280**, 560–564 (1998).
17. M. Muehlhofer, T. Strassner, W. A. Herrmann, *Angew. Chem. Int. Ed.* **41**, 1745–1747 (2002).
18. T. Strassner, M. Muehlhofer, A. Zeller, E. Herdtweck, W. A. Herrmann, *J. Organomet. Chem.* **689**, 1418–1424 (2004).
19. S. Ahrens, A. Zeller, M. Taige, T. Strassner, *Organometallics* **25**, 5409–5415 (2006).
20. J. F. Hartwig, *Acc. Chem. Res.* **45**, 864–873 (2012).
21. J. F. Hartwig *et al.*, *J. Am. Chem. Soc.* **127**, 2538–2552 (2005).
22. H. Chen, S. Schlecht, T. C. Semple, J. F. Hartwig, *Science* **287**, 1995–1997 (2000).
23. Z. An, X. Pan, X. Liu, X. Han, X. Bao, *J. Am. Chem. Soc.* **128**, 16028–16029 (2006).
24. G. J. Hutchings, M. S. Scurrell, J. R. Woodhouse, *Chem. Soc. Rev.* **18**, 251–283 (1989).
25. C. Hammond *et al.*, *Angew. Chem. Int. Ed.* **51**, 5129–5133 (2012).
26. P. Vanelderen, J. Vancauwenbergh, B. F. Sels, R. A. Schoonheydt, *Coord. Chem. Rev.* **257**, 483–494 (2013).
27. M. N. Vargaftik, I. P. Stolarov, I. I. Moiseev, *J. Chem. Soc. Chem. Commun.* **1990**, 1049–1050 (1990).

28. I. P. Stolarov, M. N. Vargaftik, D. I. Shishkin, I. I. Moiseev, *J. Chem. Soc. Chem. Commun.* **1991**, 938–939 (1991).
29. A. J. Bard, R. Parsons, J. Jordan, *Standard Potentials in Aqueous Solution* (International Union of Pure and Applied Chemistry, New York, 1985).
30. M. Ahlquist, R. A. Periana, W. A. Goddard Iii, *Chem. Commun. (Camb.)* **17**, 2373–2375 (2009).
31. F. Basolo, R. G. Pearson, *Mechanisms of Inorganic Reactions* (Wiley, New York, ed. 2, 1967).
32. R. G. Peterson, *Hard and Soft Acids and Bases* (Dowden, Hutchinson and Ross, Stroudsburg, PA, 1973).
33. H. Kurosawa, R. Okawara, *J. Organomet. Chem.* **10**, 211–217 (1967).
34. T. Fujii, K. Funahashi, I. Hirose, U.S. patent 3399956 (1968)
35. R. A. Johnson, U.S. patent 4113756 (1978)
36. R. A. Johnson, U.S. patent 4192814 (1980)

Acknowledgments: This work was supported as part of the Center for Catalytic Hydrocarbon Functionalization, an Energy Frontier Research Center Funded by the U.S. Department of Energy, Office of Science, Office of Basic Energy Sciences, under award DE-SC0001298 (to R.A.P. and D.H.E). D.H.E. thanks the BYU Fulton Supercomputing Lab. We also thank S. Burt (BYU) for assistance with Tl NMR. Several provisional and one nonprovisional patents have been filed (applications PCT/US2014/018175, 61/768,715, 61/862,715, 61/862,723, and 61/862,731).

Supplementary Materials
www.sciencemag.org/content/343/6176/1232/suppl/DC1
Materials and Methods
Figs. S1 to S9
Tables S1 to S3
Schemes S1 to S4
References (*37*–*47*)

5 December 2013; accepted 19 February 2014
10.1126/science.1249357

Changes in Seismic Anisotropy Shed Light on the Nature of the Gutenberg Discontinuity

Caroline Beghein,[1]* Kaiqing Yuan,[1] Nicholas Schmerr,[2] Zheng Xing[1]

The boundary between the lithosphere and asthenosphere is associated with a platewide high–seismic velocity "lid" overlying lowered velocities, consistent with thermal models. Seismic body waves also intermittently detect a sharp velocity reduction at similar depths, the Gutenberg (G) discontinuity, which cannot be explained by temperature alone. We compared an anisotropic tomography model with detections of the G to evaluate their context and relation to the lithosphere-asthenosphere boundary (LAB). We find that the G is primarily associated with vertical changes in azimuthal anisotropy and lies above a thermally controlled LAB, implying that the two are not equivalent interfaces. The origin of the G is a result of frozen-in lithospheric structures, regional compositional variations of the mantle, or dynamically perturbed LAB.

Plate tectonic theory describes a strong and rigid lithospheric "lid" that translates coherently atop a weaker and more deformable convecting asthenosphere. Determining the depth and pervasiveness of the interface between these two layers, known as the lithosphere-asthenosphere boundary (LAB), is key for understanding the formation, evolution, and thermochemical properties of plates and associated tectonics. The exact compositional and thermal mechanisms that control this rheological division remain enigmatic, but seismological imaging of anisotropy—the directional dependence of seismic wave velocity—across the upper mantle provides an essential tool for interrogating the transition in material properties across the LAB.

Seismological interrogations of the oceanic upper mantle beneath the Pacific Ocean find evidence for a sharp drop in seismic velocity, known as the Gutenberg (G) discontinuity (*1*), at 40- to 100-km depth. The depth of the G roughly coincides with the top of a low-velocity zone (LVZ) and may be the seismological expression of the LAB. However, correlating G depth with plate age and distance to mid-ocean ridges has not produced a unifying interpretation of the relationship between the G and the LAB (*2*–*6*). This has led to several alternative hypotheses for the origin of the G, including partial melt lenses in the asthenosphere (*3*), hydrogen depletion of olivine from decompression melting beneath mid-oceanic ridges (*7*, *8*), frequency-dependent attenuation effects reducing the shear modulus in the presence of mantle hydration (*9*), and dynamical melt-producing processes to explain the strong regional variations in G reflectivity from *SS* precursor data (*5*, *10*).

To improve our understanding of how isotropic and anisotropic velocity models relate to the observations of seismic discontinuities, we modeled the three-dimensional isotropic and anisotropic structure of the upper mantle beneath the Pacific Basin (Fig. 1) using a global data set of surface wave phase velocity maps (*11*, *12*). The dispersive properties of surface waves make them ideal to put depth constraints on seismic anisotropy and velocity, and the use of higher-mode surface waves to model azimuthal anisotropy provides sensitivity throughout the upper mantle (fig. S1). The detection of changes in seismic anisotropy has been successfully used to identify layering in the mantle, variations in LAB depth beneath continents and oceans (*13*, *14*), and chemical stratification within the lithosphere under the North American craton (*14*). Here we focus on anisotropy under the Pacific Plate, which is well sampled by surface waves and therefore constitutes a natural laboratory to constrain the evolution and cooling history of the oceanic lithosphere. The surface wave anisotropy results are compared to a large data set of high-frequency *SS* precursors that highlight the G (*5*).

Our models show a stratified upper mantle under the Pacific Ocean and a correlation between the boundaries of these layers and the location of observed seismic discontinuities (Fig. 2). The top layer (layer 1) is defined by a poor alignment between V_{SV} fast axes direction and the absolute plate motion (APM) (*15*), and the underlying layer (layer 2) by a better alignment with the APM. Layer 1 is also characterized by high seismic velocities away from ocean ridges [4 to 5% with respect to our reference model (*16*)], and its thickness increases with crustal age, similar to past surface wave studies (*13*, *17*–*19*). Furthermore, layer 1 is associated with 1 to 2% radial anisotropy with $V_{SV} > V_{SH}$, and azimuthal anisotropy amplitudes of 1 to 2%. This fast V_{SV} direction roughly follows the orientation of ocean floor fracture zones at 50-km depth near ridges, around 80-km depth for ocean ages between 80 and 120 million years ago (Ma), and at 100-km depth under old oceanic plates (Fig. 1). Ocean floor fracture zones are temporally stable features that record plate motion path and can thus be used as proxy for the paleospreading directions. Layer 2 has lower *S*-wave velocity (–5% relative perturbations), strong radial anisotropy (5%) with $V_{SH} > V_{SV}$, and 3% azimuthal anisotropy with, by definition, fast axes subparallel to the APM (<30° deviation from APM).

On the basis of the above seismological observations, we define the LAB in our models as the dipping interface between these two layers. The strong anisotropy of layer 2 suggests alignment of olivine fast axes with mantle flow direction associated with plate motion that can occur in the deformable asthenosphere by dislocation creep (*20*) or diffusion creep (*21*). Olivine lattice-preferred orientation (LPO) formed by mantle flow–induced shear strain in the dislocation creep regime is consistent with a low-viscosity asthenosphere (*22*) and a flow channel coincident with a low-velocity zone (*23*). The thickness of our tomographically defined layer 1 increases with plate age, following the 900° to 1100°C isotherms in a half-space cooling (HSC) model (black lines, Fig. 2). Combined with elevated seismic velocities, layer 1 is therefore consistent with cold lithosphere that has a thermally controlled thickness and implies that the LAB is a temperature-related phenomenon. Furthermore, the alignment of the V_{SV} fast axes with the fossil spreading direction in layer 1 is consistent with LPO and the frozen-in record

[1]Department of Earth, Planetary, and Space Sciences, University of California, Los Angeles, 595 Charles Young Drive East, Box 951567, Los Angeles, CA 90095–1567, USA. [2]Department of Geology, University of Maryland, College Park, MD 20742, USA.
*Corresponding author. E-mail: cbeghein@ucla.edu

Science
AAAS

Main-Group Compounds Selectively Oxidize Mixtures of Methane, Ethane, and Propane to Alcohol Esters

Brian G. Hashiguchi *et al.*

Science **343**, 1232 (2014);
DOI: 10.1126/science.1249357

Science (print ISSN 0036-8075; online ISSN 1095-9203) is published weekly, except the last week in December, by the American Association for the Advancement of Science, 1200 New York Avenue NW, Washington, DC 20005.